



Available online at www.sciencedirect.com

ScienceDirect

journal homepage: www.keaipublishing.com/foar



SOUTHEAST UNIVERSITY

RESEARCH ARTICLE

Urban traffic modeling and pattern detection using online map vendors and self-organizing maps



Zifeng Guo ^{a,*}, Biao Li ^b, Ludger Hovestadt ^a

^a Department of Architecture, Swiss Federal Institute of Technology Zurich (ETHZ), Zurich, 8093, Switzerland

^b School of Architecture, Southeast University, Nanjing, 210096, China

Received 29 January 2021; received in revised form 23 May 2021; accepted 23 June 2021

KEYWORDS

Urban traffic patterns;
Data-driven modeling;
Urban management;
Map vendors

Abstract Typical traffic modeling approaches, such as network-based methods and simulation models, have been shown inadequate for urban-scale studies due to the fidelity issue of models. As a go-around, data-driven models have received increasing attention recently. However, most data-driven methods have been restricted by their data source and cannot be scaled up to manage urban- and regional-scale studies. Regarding this issue, this research proposes a pipeline that collects traffic data from online map vendors to bypass data limitations for large-scale studies. The study consists of two experiments: 1) recognizing the dominant traffic patterns of cities and 2) site-specific predictions of typical traffic or the most probable locations of patterns of interests. The experiments were conducted on 32 Swiss cities using traffic data that were collected for a two-month period. The results show that dominant patterns can be extracted from the temporal traffic data, and similar patterns exist not only in various parts of a city but also in different cities. Moreover, the results reveal that a country-level lockdown decreased traffic congestions in regional highways but increased those connections near the city centers and the country borders.

© 2021 Higher Education Press Limited Company. Publishing services by Elsevier B.V. on behalf of KeAi Communications Co. Ltd. This is an open access article under the CC BY-NC-ND license (<http://creativecommons.org/licenses/by-nc-nd/4.0/>).

* Corresponding author.

E-mail address: guo@arch.ethz.ch (Z. Guo).

Peer review under responsibility of Southeast University.

1. Introduction

Traffic networks are the fundamental component of every modern city, serving as not only the infrastructure for logistics and transportation but also the landscape that shapes our impressions of different cities (Hamilton-Baillie, 2004). The study of urban traffic networks, especially the relation between traffic flow patterns and other built environment factors, has always been a core interest of urban planning and design. Such study can deepen our understanding of how cities work (e.g., Batty, 2008; Ewing et al., 2018; Wang et al., 2018) and offer a better decision-making process for urban management (e.g., Shi 2019; Ahmadzai 2020). The study of urban traffic patterns also provides valuable knowledge for urban planners and designers to integrate transportation planning better in the urban design workflow for more sustainable urban layouts (Konieva et al., 2019).

In the context of urban planning and design, the studies of traffic pattern networks typically fall into two major paradigms. The first one treats traffic networks as graphs whose analytical properties, such as the number of edges and the shortest path, are the indicators of certain real-world phenomena (e.g., Hillier et al., 1976; Bafna, 2003; Ahmadzai et al., 2019). For example, the population of the urban region around a road segment can be inferred by the number of nodes of the shortest paths between this segment and all other street segments of the city (Hillier et al., 1993). The second one considers traffic flow as a physical process that can be modeled and simulated using computers. These computer simulations are typically categorized as microscopic and macroscopic models. Microscopic models describe the dynamics of single vehicles and their interactions using agent-based (e.g., Gipps et al., 1981; Bando et al., 1995; Krajzewicz et al., 2002) or cellular-automata-based approaches (e.g., Cremer and Ludwig, 1986; Esser and Schreckenberg, 1997; Knospe et al., 2004). In these models, the micro-level interactions of vehicles can exhibit macro-level traffic patterns. In contrast to the microscopic models, macroscopic models describe traffic flows as if they were continuum flows like fluids. These models use aggregated variables, such as density and velocity, rather than the behavior of individual vehicles, to represent the traffic flows. Macroscopic models were first introduced as the kinematic wave model (Lighthill and Whitham, 1955; Richards 1956). The model was later developed into multi-class models, which differentiate different lanes and driving styles for traffic networks (e.g., Wong and Wong, 2002), and high-order models, which consider the acceleration and deceleration process of vehicles (e.g., Aw and Rascle, 2000). In addition, hybrid approaches that combine the features of micro and macro models were also proposed for realistic vehicle-level traffic simulations (e.g., Härrí et al., 2006).

Despite the intensive investigations, both paradigms show several limitations that prevent them from being suitable for urban-scale studies. First, graph-based approaches oversimplify the traffic systems and treat every city equally. They can provide certain information on traffic in different cities but not necessarily make accurate predictions about any individual city (Evans et al., 2013, 2014).

Second, graph-based approaches have also been criticized for their mathematical inconsistency through which the same urban configuration may produce completely different results (Ratti, 2004). Third, both paradigms ignore detailed factors of the built environment, such as land use and building heights, which means they treat the entire city homogeneously. Notably, this issue was not explored until recently (Sakai et al., 2019). Lastly, for traffic flow simulations, both microscopic and macroscopic models lack validation experiments. These models need to be calibrated using observational data to represent realities better than the original models. The calibration is essentially an optimization process searching for the optimal values for the model's parameters. However, the calibration process does not guarantee accurate predictions, as the selected model may not be an appropriate representation of the study areas (Rakha et al., 1996). Furthermore, the calibration process is limited by the amount of data that are available (Sewall et al., 2011). Thus, the study areas of most calibration experiments have been small regions that consist of few road segments (e.g., Härrí et al., 2006; Spiliopoulou et al., 2014; 2015; Montanino and Punzo, 2015) rather than the entire city.

To overcome the fidelity issue of simulations, data-driven approaches that take advantage of observational data have been proposed as the alternative to predefined simulation models for traffic and mobility modeling. These approaches were initially proposed as trajectory-tracing methods from measurements, such as communication time and angles within cellular networks (Zonoozi and Dassanayake, 1997). Later, the availability of growing data has emphasized the paradigm shift toward pattern recognitions and predictions. Many relevant data sources, such as mobile phone records released by service operators (e.g., Yuan and Raubal, 2012), user geolocation records from online social networks (e.g., Endarnoto et al., 2011; Noulas et al., 2012), and transaction records of public transports (e.g., Hasan et al., 2013), have been investigated. In parallel to these works, several studies for traffic pattern modeling have been conducted using the raw traffic data recorded by sensors at the links and intersections of a traffic network (e.g., Chen et al., 2006, 2008; Brunauer et al., 2018). These studies have shown that similar traffic patterns exist in different parts of a network, thus opening the possibility of imputing missing traffic data (Laña et al., 2018) and predicting future traffic patterns (Laña et al., 2019). Despite their effectiveness regarding realistic issues, existing data-driven approaches are highly dependent on their data source and cannot be easily scaled up. In addition, several restrictions still exist. First, researchers have had increasing difficulty accessing raw data, such as user trajectories, due to monopoly and privacy issues. Second, publicly released datasets are usually not up to date. Third, most publicly released datasets are still incomplete in terms of the region of interests (for example, same-quality data from multiple cities). These restrictions have become significant for urban-scale studies that emphasize the traffic aspect of cities.

In this study, we propose the use of online map vendors as an alternative to publicly released datasets for large-scale traffic modeling and pattern recognition. The study demonstrates a systematic pipeline for collecting and

processing real-time traffic data from online map vendors, conducting urban-level pattern recognitions, and performing relevant predictions, such as the typical traffic patterns of a region or typical locations for patterns of interests. Our study uses self-organizing map (SOM) as the mean of pattern recognition and prediction. Compared with other SOM-based studies that prioritize spatial patterns (e.g., Chen et al., 2006, 2008) or spatial-temporal pattern at each individual intersection (e.g., Brunauer et al., 2018), our study prioritizes temporal patterns so that the results are not restricted to certain spatial arrangement and thus become comparable among different locations. The main contributions of the study include:

- The study proposes a data-driven pipeline using online map vendors as the data source for urban-scale traffic modeling.
- The study shows that the similarity of road segments can be determined by their traffic flow patterns rather than their spatial and geometric properties. This metric of similarity applies to road segments not only from the same city, but also from different cities, thus revealing a new layer of information for urban planning and urban management.
- The study collected data before and after a country-level lockdown due to the pandemic, thus showing how such event affects the traffic behavior of cities.
- The study shows that various types of spatial and temporal predictions can be made using the recognized temporal patterns.

2. Pipeline

The pipeline of this study can be described in three steps. The first step is data collection. We used a list of geo-bounding boxes to collect geo-tagged screenshot images from Google Maps as our main data source. The screenshots were constantly taken so that each geo-bounding box corresponded to a sequence of screenshot images that represented the dynamic process of the traffic flows. The collected screenshots represented traffic congestions by rendering road segments in different colors. These colors were filtered out and merged with traffic network data collected from OpenStreetMap (OSM). At the end of the data collection process, we had a list of traffic networks containing sequential traffic flow data.

The second step is to conduct traffic pattern recognition using the collected data. For this step, we considered temporal traffic data as the training vectors and trained a SOM to detect the most typical temporal patterns. These temporal patterns were then projected back to the traffic networks for spatial analysis. The spatial distribution of temporal patterns helped us to understand the role of each part of the traffic network during the pandemic period. Furthermore, it provided a means to bring multiple cities together for comparisons.

The last step is to perform detailed traffic predictions based on the typical patterns learned in the second step. As a demonstration, we selected one city for the case study and conducted two types of predictions: the prediction of

typical traffic at specific datetimes and the most probable locations of certain traffic patterns. Apart from these two types, other variants of prediction tasks, such as asking for the most probable datetime for certain traffic patterns at specific locations, could also be made. This possibility was explained by the mechanism we used for making traffic predictions. Fig. 1 shows the complete pipeline.

3. Data collection and processing

3.1. Collecting screenshot tiles

The study extracted traffic data from the screenshot images of Google Maps. These screenshots were sampled by specifying the coordinates (longitude and latitude) and the zoom level in the URL address. The coordinates determine the location of the center pixel of the map, while the zoom level determines the spatial resolutions (meter/pixel). As Google uses 256×256 pixel tiles that were calculated by Mercator projection (Google, 2020), the spatial resolution $m(\varphi, z)$ of a pixel at latitude φ with the zoom level z can be determined by:

$$m(\varphi, z) = 2\pi R \frac{\cos \varphi}{256 * 2^z} = \pi R \frac{\cos \varphi}{2^{z+7}},$$

where R is the earth radius (6,378,137 m). The spatial resolution was used to calculate the x-y extents of the screenshots so that the screenshots were geo-tagged and could be merged with other geo-data accurately. For simplicity, we used the same φ , which corresponded to the latitude of the center point of a screenshot for all the pixels of the same screenshot.

As Google Maps only shows traffic data when the spatial resolution is sufficiently high, we collected screenshot tiles using large zoom levels and assembled the tiles to larger images for the entire city. This process was accomplished by subdividing the entire city (based on the administrative boundary) into a regular grid such that each grid cell could be fully captured by a regular display resolution (e.g., 1280×1024 pixels). The subdivision size also depended on the zoom level. A higher zoom level resulted in finer data but also more tiles. As a balance between the data quality and the speed, a zoom level of 15 was used for tile collection.

In practice, we clipped the tiles to a smaller size (e.g., 1000×800 pixels) to exclude unnecessary graphic elements of the webpage. We also generated grid cell coordinates based on a source coordinate (typically the city center) such that 1) the distance between every two adjacent coordinates equaled the size (meters) of a clipped tile and 2) the grid completely covered the bounding box of the city's administrative boundary. Both the source coordinate and the administrative boundary were obtained from the Nomination API (<https://nominatim.openstreetmap.org/>) of OSM. The formula for calculating a destination coordinate from a source is given as

$$\varphi_2 = \cos \frac{d}{R} \sin \varphi_1 + \sin \frac{d}{R} \cos \varphi_1 \cos \alpha,$$

$$\lambda_2 = \lambda_1 + \text{acos} \frac{\cos \alpha - \sin \varphi_1 \sin \varphi_2}{\cos \varphi_1 \cos \varphi_2},$$

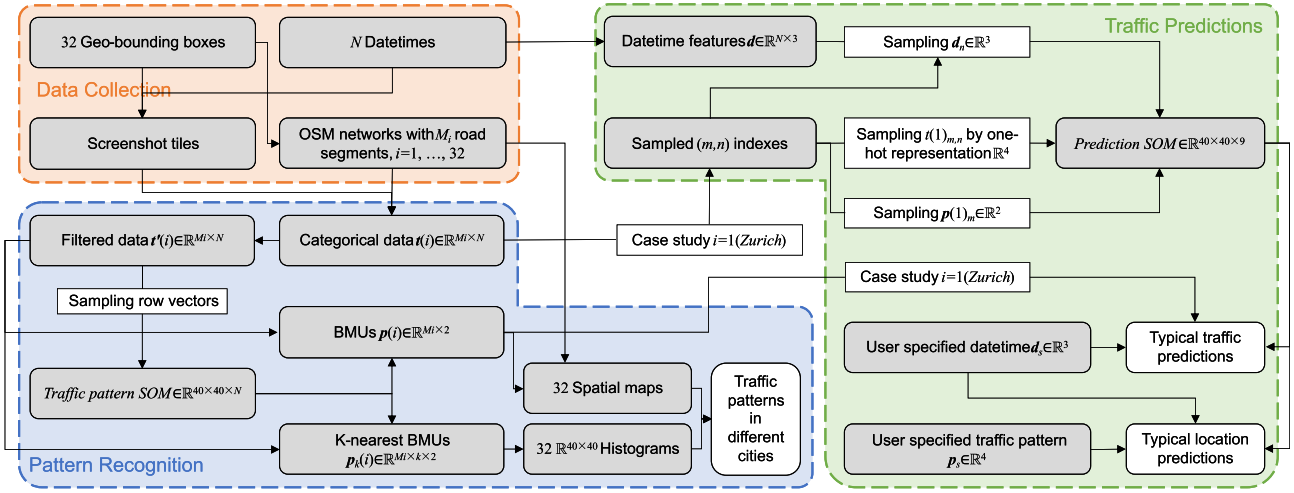


Fig. 1 The schematic diagram of the study.

where d is the great-circle distance between source and destination. R is the earth radius, and α is the azimuth. In addition, φ_1, λ_1 and φ_2, λ_2 are the latitude-longitude of the source and destination, respectively.

This data collection method was applied to the 32 most populated cities in Switzerland. These cities were selected as they have a population greater than 20,000. The data collection was performed in 10-min intervals from Feb. 26th, 2020 to Apr. 12th, 2020. We selected this sampling frequency as a balance between the temporal resolution of the data and the amount of computational resource required.

3.2. Overlapping screenshot tiles with traffic networks

The road segments of the screenshot images were rendered in four different colors that represent the four categories of traffic flow velocities. As previous studies had revealed a negative relationship between the flow velocity and density (Edie, 1965), these colors could be interpreted as the density of the traffic (i.e., the number of vehicles per unit road segment) as well as the level of traffic congestions. However, as Google did not disclose the exact algorithm of how these colors were produced, the exact velocity and density data from the screenshots could not be retrieved. Therefore, we followed Google's four categories of traffic velocities and represented the categories as integers (green as 0, orange as 1, red as 2, and dark red as 3). These categories were called the *traffic congestion levels*.

The four categories of road segments were extracted from the screenshots as scattered pixels using color filtering. However, the extracted pixels could not be directly used as the final data for further experiments because 1) some pixels might represent irrelevant visual elements, such as buildings, texts, and icons, that were rendered by similar colors and 2) no pixel would be extracted from road segments where traffic data were temporarily unavailable. Although Google did not disclose any details regarding their algorithm, a reasonable assumption was that the traffic data were determined on

the basis of the quantity and velocity of smartphones using Google Maps for navigation (Weckert, 2020). Therefore, no-data road segments likely had the lowest traffic density (Fig. 2). On the basis of these two reasons, we decided to match the filtered pixels to the traffic networks to produce the final data for further experiments.

The process of matching the filtered pixels to a traffic network can be described as follows. First, a traffic network that had the same x-y extent of the assembled screenshots was collected from OSM. Then, the long road segments of the traffic network were subdivided into shorter segments to increase the spatial resolution of each road segment, as a long segment may have different traffic conditions at different ends. In our experiment, we uniformly subdivided segments that were longer than 50 m. Then, we searched for the nearest extracted pixel of each subdivided road segment within a threshold distance. The color of the found pixel was used as the categorical traffic data of the road segment. If no pixel was found, a default value of 0, which represents the lowest traffic density, was assigned to the corresponding road segments.

3.3. Postprocessing

The categorical traffic data of the resulting traffic networks consisted of a few missing datetimes (a maximum 30-min gap) due to temporary Internet failure. The error was fixed by filling the missing datetimes with the values of the nearest available datetimes. In addition, we ignored different lanes and travel directions of the road segments for simplicity. These factors could be included in future works by combining more detailed traffic networks with screenshots of higher pixel resolutions.

The matching and post-processing processes were conducted for each traffic network on all available screenshot tiles, thus resulting in 32 traffic networks that contained two-month sequential traffic data. For each traffic network, the resulting traffic data can be represented by a matrix $t(i) \in \mathbb{R}^{M_i \times N}$, where i is the index of the traffic network, M_i is the total number of road segments of the i -th network, and N represents the total number of datetimes.

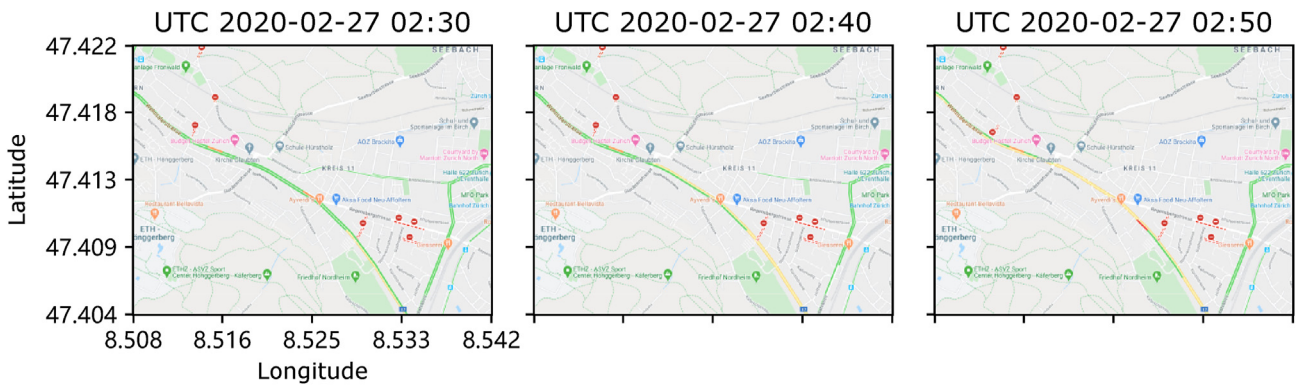


Fig. 2 A road segment turned from has-data to no-data.

Hence, matrix element $t(i)_{m,n}$ represents the traffic congestion level of the m -th road segment at the n -th datetime. Notably, $t(i)_{m,n} \in \{0, 1, 2, 3\}$, which corresponds to the four traffic congestion categories of Google Maps. For convenience, we replaced index i with the city name when referring to the traffic data from a specific city. For example, $t(\text{Zurich})$ represents the processed traffic data of the city of Zurich.

The collected traffic congestion levels t_m were discrete categories of traffic conditions. To create a continuous view of the traffic flow and to represent the status situated among different categories, we used Gaussian filtering to postprocess the collected integers. This process can be described as

$$t(i)'_{m,n} = \frac{\sum_{k=-K}^K t(i)_{m,n+k} g(k)}{\sum_{k=-K}^K g(k)},$$

where $t(i)'_{m,n}$ is the filtered traffic data of the i -th network. g is the Gaussian function with $\sigma = 4$ and $\mu = 0$, and K is the radius of the truncated discrete Gaussian kernel. We used $K = 12$ for the postprocessing.

4. Traffic flow pattern detection

The first experiment focuses on the traffic flow pattern of the case study cities. The pipeline of this experiment can be described as follows. First, we prioritized temporal traffic data and randomly sampled row vectors $t'_{m \in \mathbb{R}^N}$ from all filtered traffic data matrices $t'(i) \in \mathbb{R}^{M \times N}$ with a sampling ratio of 10%. The sampling results are denoted as $t' = \{t'_m | m = 1, \dots, M\}$, where M is the total number of samples. Then, the sampled vectors were used to conduct an unsupervised learning process to extract typical temporal traffic patterns. Afterward, the extracted patterns were projected to the road networks to study the spatial distribution of patterns. We prioritized temporal patterns (row vectors) because, unlike other works, such as Chen et al. (2006, 2008), that prioritized spatial patterns (column vectors), the recognized temporal patterns were not restricted to a certain spatial arrangement. Thus, the patterns were comparable among different locations. This pattern-level comparability brought an interesting direction for urban- and traffic-related studies, as we could compare different cities in terms of their traffic behaviors.

4.1. Self-organizing map and its training process

The experiment used SOM for temporal traffic pattern detection. SOM is a type of artificial neural network that was proposed by Kohonen (1982) for unsupervised learning. A SOM consists of a collection of nodes that are organized in a regular grid. Each node corresponds to a weight vector that serves as the cluster center. The training of a SOM uses a competitive learning strategy in which the training samples are successively presented to the network to modify the network's weight vectors. Each training sample always modifies a subset of the weight vectors such that the Euclidean distance between the training sample and the subset decreases. The subset is determined by a neighborhood radius and the x - y position of the training sample's best-matching unit (BMU)—the node whose weight vector has the minimum Euclidean distance to the training sample. Given that each training sample corresponds to different subsets, the training is a competitive process among different training samples. Each complete round of processing all training samples is called an epoch. In addition, a SOM is typically trained for multiple epochs, and after each epoch, the neighboring radius decreases.

This competitive learning process was implemented by a batch-training method (Takatsuka and Bui, 2010). Specifically, let D represents the dimensionality of the weight vectors, $x_i \in \mathbb{R}^D$ represents the i -th training sample, $u_i \in \mathbb{R}^2$ represents the node position of the BMU of x_i , $w_j \in \mathbb{R}^D$ represents the weight vector of j -th node, and $v_j \in \mathbb{R}^2$ represents the position of the j -th node. The formula for updating the weight vector of the j -th node can be written as

$$w_j = \frac{\sum_i x_i h(||u_i - v_j||)}{\sum_i h(||u_i - v_j||)},$$

where h is the neighborhood function typically defined as a Gaussian function. The standard deviation σ of the Gaussian function serves as the neighborhood radius that linearly decreases to 1 as the training epoch increases. The batch-training method modifies all weight vectors simultaneously, thus accelerating the training process.

4.2. Traffic-pattern recognition using SOM

The temporal traffic patterns of the case study cities were obtained by training a SOM (called the *traffic-pattern SOM*)

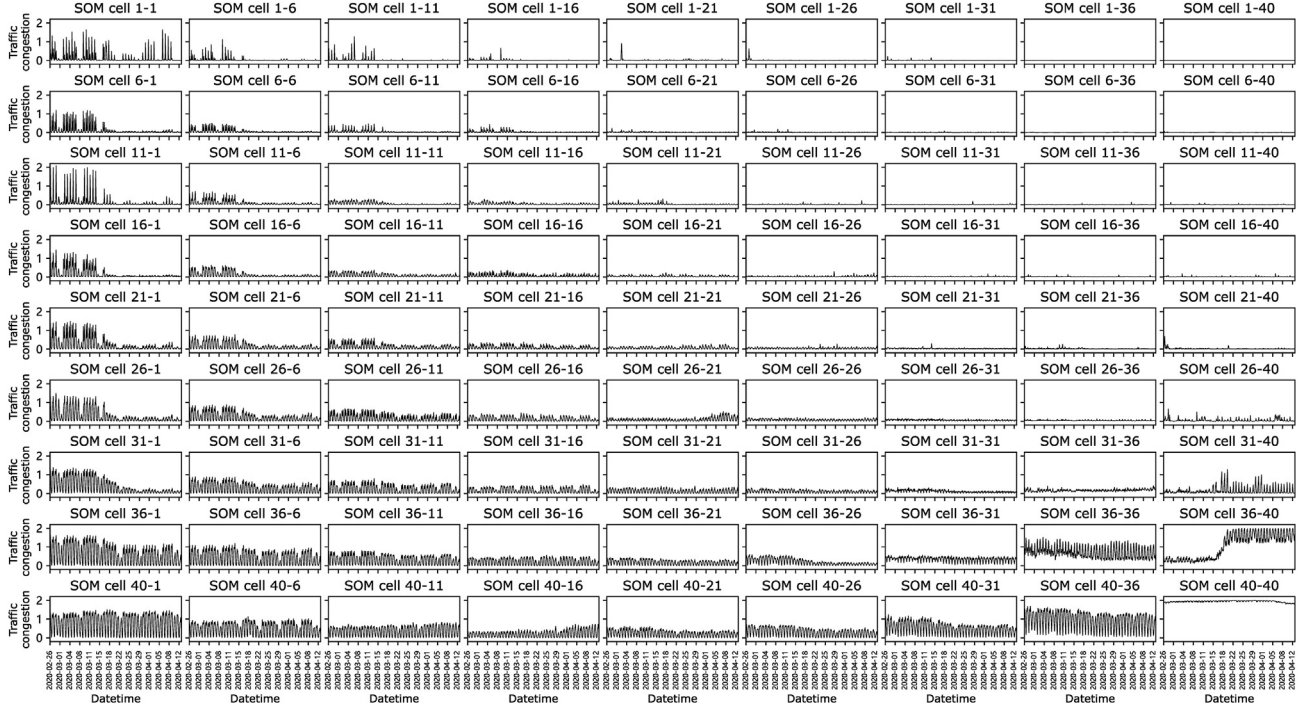


Fig. 3 The *traffic-pattern SOM* rendered as the temporal traffic plots of subsampled cells.

with sampled traffic vectors t' using the method described in section 4.1. In our experiment, the *traffic-pattern SOM* consists of 40×40 nodes as a balance between the precision and computational cost.

The trained *traffic-pattern SOM* exhibits a smooth-changing pattern between the neighboring nodes. Thus, it can be visualized for visual inspections (Fig. 3). However, to differentiate various temporal patterns further, we conducted another iteration of clustering using the K-means algorithm to group the weight vectors of the *traffic-pattern SOM* into six clusters. As shown in Fig. 4, each cluster corresponds to a different area of the SOM as well as a different temporal traffic pattern. Specifically, cluster 0 shows a pattern in which the traffic congestions are minimum regardless of the datetimes. Cluster 3 shows patterns with a significant increase in traffic congestions after lockdown. Clusters 2 and 4 demonstrate a significant

decrease in traffic congestions after the lockdown. The difference between these two clusters is the average traffic congestion levels. Clusters 1 and 5 show a slight traffic congestion decrease after lockdown. However, the differences are not as significant as in other clusters.

The *traffic-pattern SOM* can be interpreted as a dimension reduction of $\mathbb{R}^N \rightarrow \mathbb{R}^2$, which maps a temporal traffic vector to an x-y position by asking the vector's BMU. This reduction is due to the SOM's essential property of topology preservation in which similar traffic vectors correspond to similar BMU positions. This property allows us to study the typical traffic pattern of a city by visualizing its traffic networks based on the BMU's positions. For example, Fig. 5 shows the spatial distribution of temporal traffic patterns in Zurich obtained by asking the BMUs of $t_{(\text{Zurich})}'$. The distribution clearly demonstrates that different parts of the traffic network are dominated by different temporal

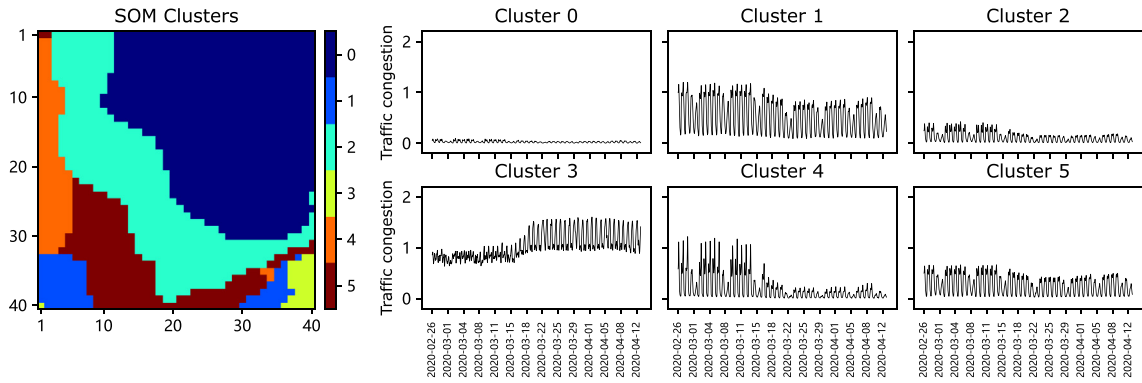


Fig. 4 Six typical patterns detected from the *traffic-pattern SOM*.

patterns. Specifically, most highways are colored in blue, which corresponds to the SOM nodes between cluster 0 and cluster 4. This distribution suggests that the lockdown reduces the traffic flows on highways. In contrast, roads near the city center are colored in yellow, which corresponds to clusters 3 and 5 and suggesting that traffic flow increased during the lockdown period. Besides these two areas, many road segments near the road intersections are colored in purple, suggesting that these road segments were heavily occupied before and after the lockdown. Lastly, most areas of the city are colored in cyan, suggesting that the impact of traffic congestions and the lockdown to these areas were minimum. The spatial distribution of temporal traffic patterns of other cities is shown in the appendix.

4.3. Traffic pattern distributions in different cities

As mentioned, we prioritized temporal traffic data so that the analysis would not be limited to specific spatial configurations, thus allowing us to compare different locations from the perspective of traffic patterns. In our experiment, we projected a traffic network on the traffic-pattern SOM by first determining the nearest k BMUs $p_k(i) \in \mathbb{R}^{M_i \times k \times 2}$ for each row vector of the traffic data. Then, we calculated the frequencies of all BMU positions. This operation could produce a 40×40 matrix for each traffic network, which represented the frequency of BMUs located at each of the 40×40 SOM nodes. We applied this operation to all the traffic networks with $k = 10$, thus resulting in 32 matrices (histograms).

The 32 matrices were entry-wise normalized so that the matrix elements of each entry had the mean of 0 and standard deviation of 1. As a result, each matrix showed the BMU distributions relative to other matrices instead of the absolute number of the distributions. The normalized 32 matrices are shown in Fig. 6. As seen, small cities, including Wetzikon, Baar, Frauenfeld, and Kreuzlingen, tended to have more BMUs distributed on the diagonal nodes from top right to bottom

left. In contrast, large cities, including Zurich, Geneva, Basel, and Lausanne, tended to have more BMUs distributed on the top left and bottom right corners. This outcome suggested that cities with similar size and populations tended to have similar traffic “behavior,” and smaller cities were less influenced than larger cities by the country-level lockdown in terms of the temporal change of traffic volumes. Another noticeable feature was that cities (such as Basel and Kreuzlingen) that are close to the border of different countries had significantly more BMUs distributed in cluster 3 (more traffic congestions after lockdown) than other cities. By comparing the spatial rendering of the corresponding cities (see Appendix), we found that the main contributors of this phenomenon were the road segments that cross the country border. The only exception was Geneva, where the road segments of similar temporal patterns were mainly located in the city center (Appendix). Lastly, we noticed that Bellinzona and Sion had a similar hotspot that was significantly higher than that of other cities. By comparing with the spatial rendering, the corresponding locations of this hotspot were mostly highways, thus suggesting that the highways in these two cities were less occupied than those in other places, such as Zurich, Geneva, and Basel.

5. Expected traffic congestions

The second experiment involved the prediction of expected traffic congestion levels at a specific datetime in different locations and the most probable locations for certain traffic patterns at a given datetime. The experiment focused on the repetitive traffic patterns that existed in long-term observations (i.e., the typical traffic of any datetime within a week) rather than a precise traffic forecast for the incoming days. The result of the experiments could assist traffic-related applications, such as predicting the noise and air pollution level caused by traffic, searching for the most probable locations for field investigations, or determining the suitable time for road constructions.

5.1. Training a prediction SOM

The experiment used a city-specific SOM (called the *prediction SOM*) for traffic predictions. The *prediction SOM* was trained with vectors that contained the information of road segments, datetimes, and traffic. These vectors were produced for a specific traffic network (the i -th network) using the following steps. First, we mapped all road segments (the row vectors of matrix $t'(i) \in \mathbb{R}^{M_i \times N}$) to their BMUs on the *traffic-pattern SOM*. The resulting BMU positions (rescaled to $[0, 1]$) were denoted as a matrix $p(i) \in \mathbb{R}^{M_i \times 2}$. Second, we calculated the *time-of-day* (mapping 00:00 to 23:59 to the range of $[0, 1]$), the *day-of-week* (mapping Monday to Sunday to the range of $[0, 1]$), and the *if-lockdown* (0 for no, and 1 for yes) values for all datetimes. This calculation produced a matrix $d \in \mathbb{R}^{N \times 3}$ in which each row vector corresponded to a specific datetime. Then, we randomly sampled a collection of (m, n) indexes for the matrix $t'(i)$. Finally, for each pair of sampled indexes (m, n) , we produced a training vector by concatenating $p(i)_m$, d_n , and the one-hot representation of $t(i)_{m,n}$. In our experiment, 100,000 pairs of (m, n) indexes were sampled as the

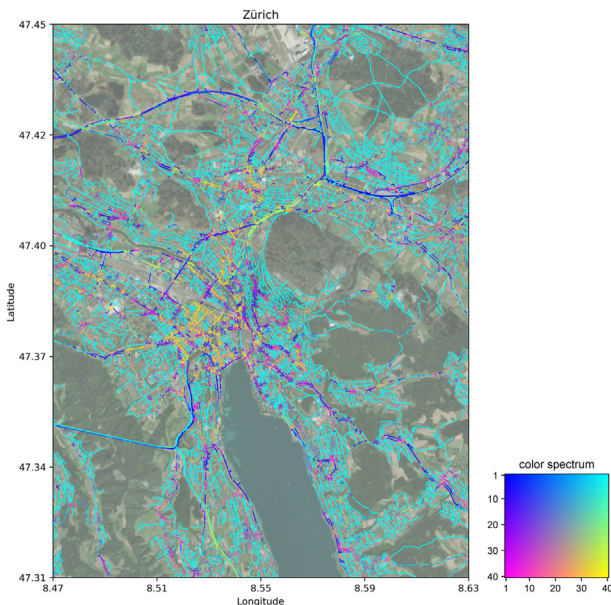


Fig. 5 Traffic network rendered by temporal patterns (left) using the color spectrum for the BMUs (right).

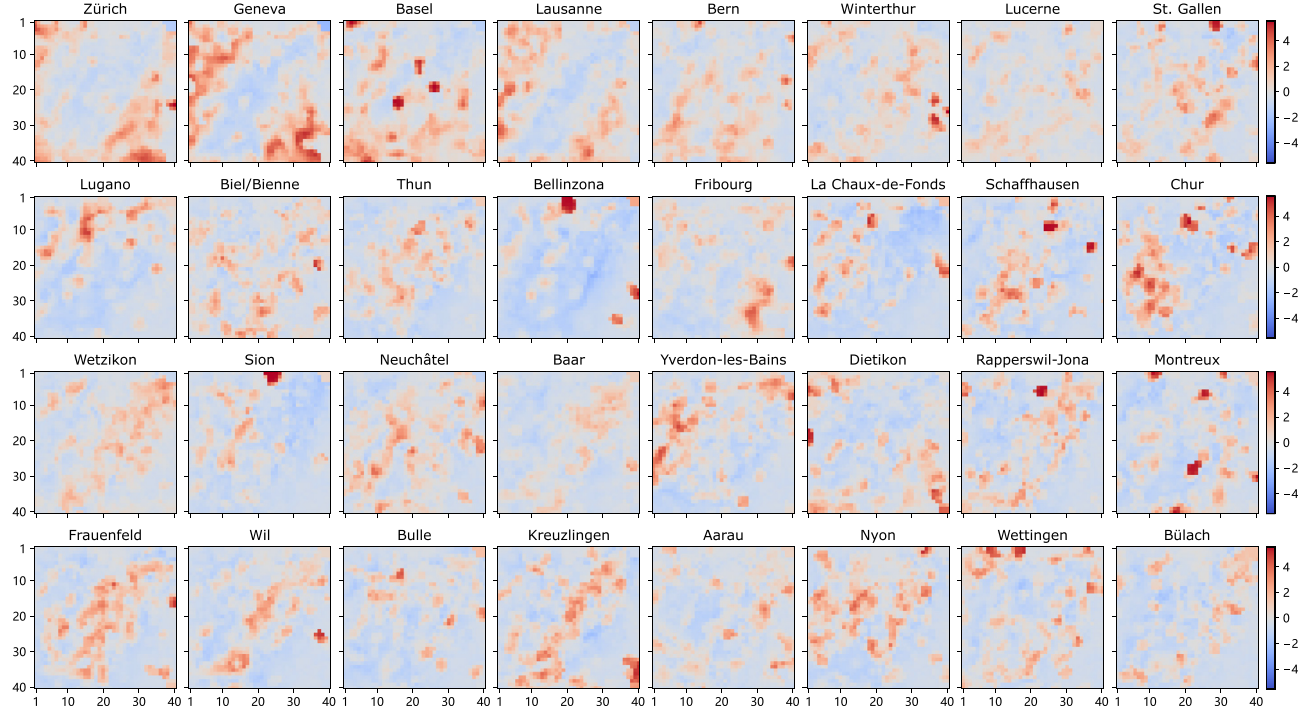


Fig. 6 The distribution of the typical traffic patterns in the 32 case study cities.

training data, and 30,000 pairs were sampled as the test data. In addition, the (m, n) indexes that existed in the training data did not exist in the test data, and vice versa. The *prediction SOM* was trained with training data only. A visualization of the trained SOM is shown in Fig. 7.

5.2. Predicting the expected traffic congestions

The prediction of the expected traffic congestions was made by feeding the *prediction SOM* with query vectors that had less dimensionality than the SOM's weight vectors. The core idea of this process is to obtain the BMUs with limited vector dimensions. More specifically, let $D_1 + D_2$ represents the dimensionality of the weight vectors of the SOM; a BMU can be obtained by calculating the Euclidean

distances between a D_1 -dimensional query vector and the first D_1 dimensions of the SOM's weight vectors. Then, the BMU's remaining D_2 dimensions serve as the prediction results. In practice, instead of using one BMU node, we can use the K-nearest SOM nodes to estimate the final prediction as, for example, the average of the obtained weight vectors. In addition, the selection of the dimensionality of the query vectors can be arbitrary, thus allowing different types of predictions to be made using the same SOM.

In the case of predicting the expected traffic congestions for the i -th network, we first specified datetime information $d_s \in \mathbb{R}^3$ and then produced query vectors $q(i) = \{p(i)_m \parallel d_s \mid m = 1, \dots, M_i\}$ for all road segments of the network. The symbol \parallel denoted the concatenation of two vectors. The query vectors $q(i)$ was fed to the

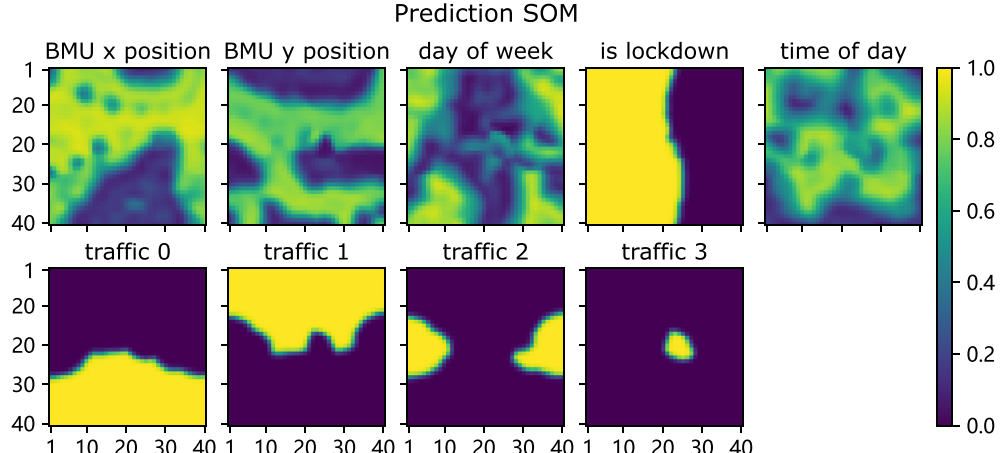


Fig. 7 The *Prediction SOM* rendered by each dimension of its weight vectors.

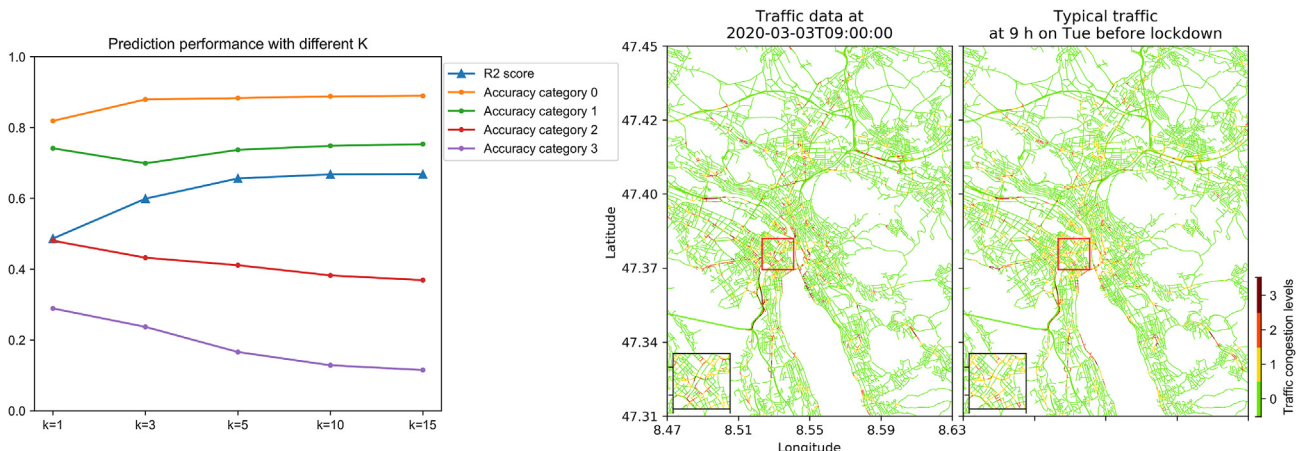


Fig. 8 The R2 score and the categorical accuracy of the prediction SOM (left) and a spatial comparison between the ground truth and the estimation (right).

prediction SOM from which $K = 5$ nearest weight vectors were returned, thus resulting in $M_i \times 5$ vectors. The returned weight vectors were averaged to M_i vectors that correspond to M_i road segments. The last four dimensions of the averaged vectors were the probabilities of the four traffic congestion levels. Based on the obtained four probabilities, the typical traffic could be derived as the discrete *traffic congestion level* by asking the dimension that gave the maximum probability (i.e., argmax operation). In addition to the discrete categories, the traffic could also be estimated as continuous values by a weighted sum operation. Specifically, $w_m = [w_{m,0}, w_{m,1}, w_{m,2}, w_{m,3}]$ provided the last four dimensions of the averaged weight vector of the m -th road segment; the traffic prediction of this road segment was obtained by $\sum_{i=0}^4 i w_{m,i}$.

The performance of the prediction SOM was validated using test data. The validation was conducted by comparing the ground truth with the traffic estimation obtained with different K nearest weight vectors. The performance was measured by 1) the prediction accuracy of the discrete

categories, and 2) the R2 value of the continuous estimation. R2 value was used because the prediction error needed to depend on categories. A misclassification between categories 0 and 1 was considered more accurate than between categories 0 and 3. The validation results are shown in Fig. 8. The increasing R2 score suggested that the accuracy was high when using multiple nearest weight vectors. Meanwhile, as K increased, the prediction was more accurate for categories 0 and 1 while less accurate for categories 2 and 3. This outcome indicated that heavy traffic congestions were detailed temporal patterns that could not be preserved by averaging multiple vectors. An example of $K = 5$ is shown on the right side of Fig. 8.

Fig. 9 shows four examples of the expected traffic congestion predictions of the city of Zurich. The first example suggests that the area is likely to face traffic congestions on highways and near city centers on Friday afternoon. Meanwhile, the second example shows a significant traffic density drop on highways and major roads due to the lockdown. Traffic patterns at different hours of the same day and on different days are shown in the third and

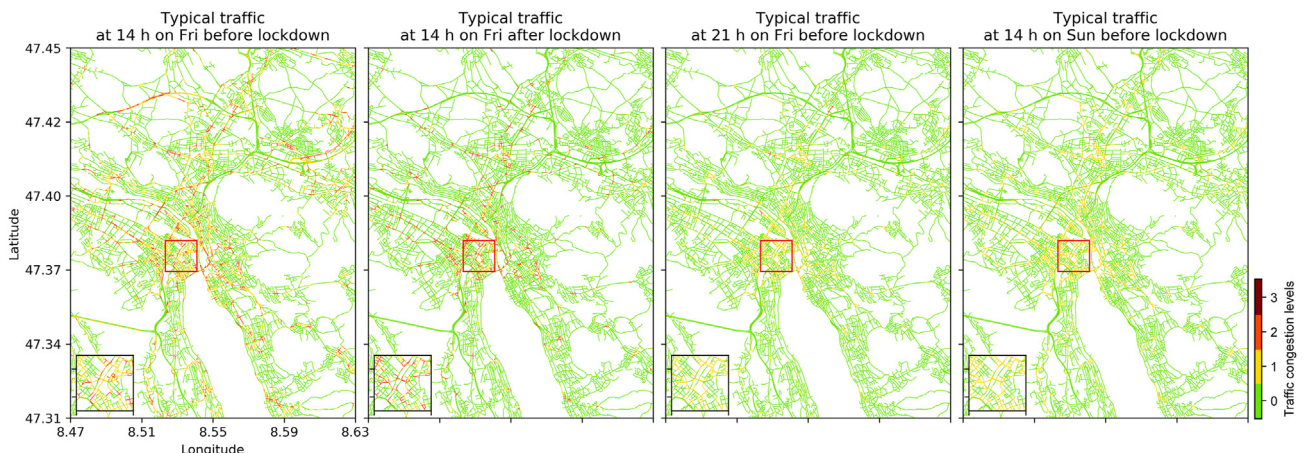


Fig. 9 Typical traffic predictions 1) at the same hour before and after lockdown (first and second); 2) at different hours (first and third); and 3) on different days (first and last).

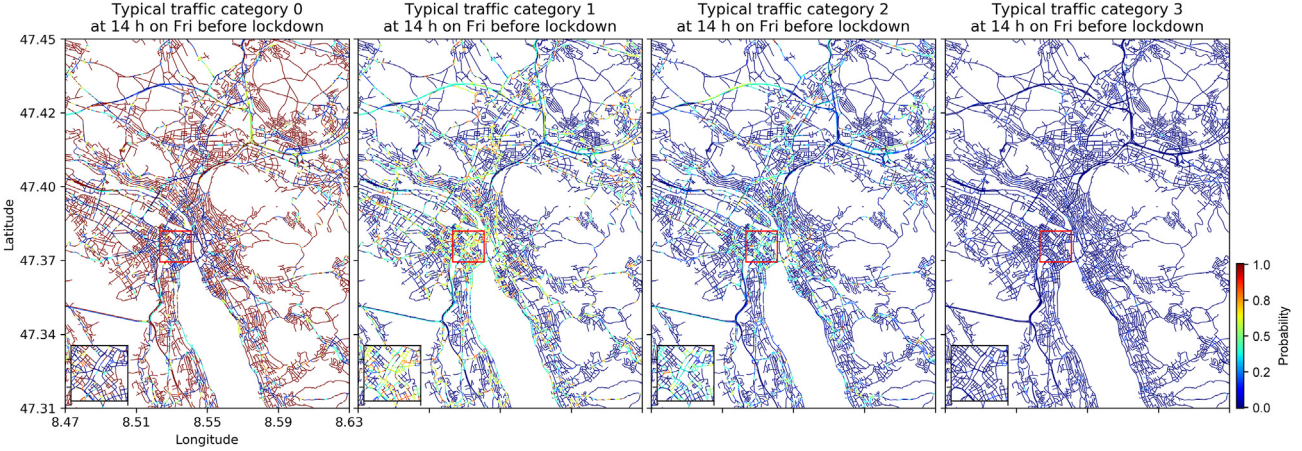


Fig. 10 The probabilities of the four traffic congestion levels, corresponding to of the first case in Fig. 9.

fourth examples, respectively. Fig. 10 presents the probabilities of the four traffic congestion levels from which the first example of Fig. 9 was calculated.

5.3. Predicting the most probable locations of certain traffic patterns

As mentioned, the dimensionalities of the query vectors can be arbitrarily selected. Hence, another meaningful prediction that can be generated with the *prediction SOM* is the most probable locations of given traffic patterns. More specifically, the query vectors for this experiment consisted of user-specified datetime information $d_s \in \mathbb{R}^3$ and one-hot traffic information $t_s \in \mathbb{R}^4$ that were specified by the user. The specified information was concatenated and fed to the *prediction SOM* to obtain the most relevant BMU positions. The obtained positions were used to determine the most probable road segments where the queried traffic pattern might occur. This information would be useful for certain scenarios, such as finding the ideal places for certain field investments and comparing the traffic flow characteristics of different cities.

In the experiment, we used a minimum $K = 5$ nearest nodes from the *prediction SOM* to obtain the BMU positions on the *traffic-pattern SOM*. The *prediction SOM* would 1) return more than five weight vectors if the Euclidean distances between the weight vectors and the query vector were below a given threshold (set to 0.05) or 2) return exactly five weight vectors otherwise. The first two dimensions of the returned weight vectors were taken as the obtained BMU positions. In addition to these acquired positions, the Euclidean distances between the weight vectors and the query vector were preserved as well. $l_k \in \mathbb{R}$ and $p_k \in \mathbb{R}^2$ denote the preserved Euclidean distances and the obtained BMU positions, respectively, in which $k \geq 5$. Then, for the m -th road segment of the i -th traffic network, a confidence value $c(i)_m$ was calculated as $c(i)_m = 1/\exp(l_j + \|p_j - p(i)_m\|)$, where $j = \arg \min_k \|p_k - p(i)_m\|$. This confidence value indicates whether 1) the queried pattern matches one of the patterns that have been learned by the *prediction SOM* and 2) the obtained BMU positions p_k matches the BMU positions $p(i)_m$ of the m -th road segment. The confidence value represents how likely the queried traffic pattern occurs in the corresponding road segment.

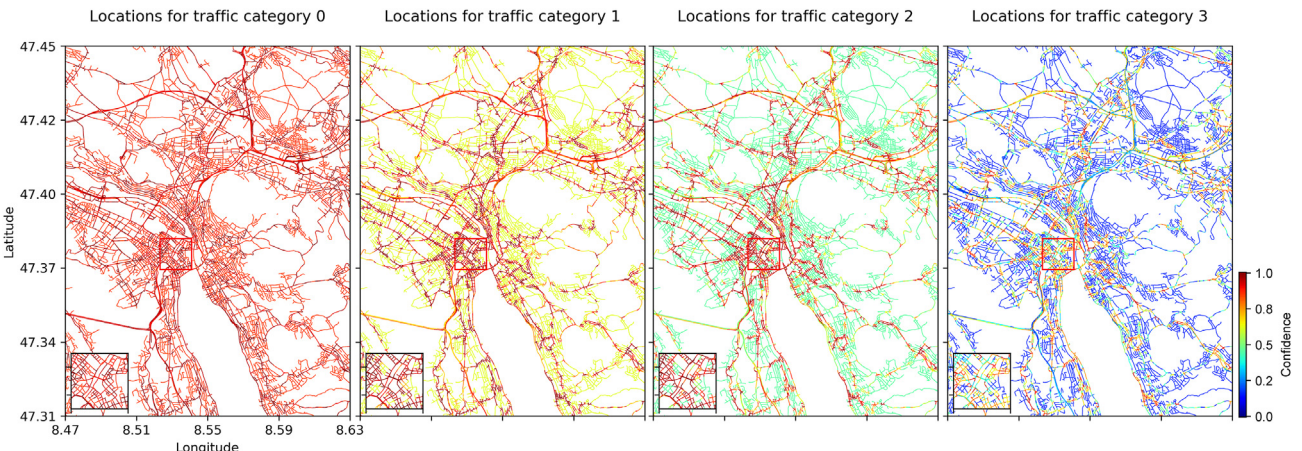


Fig. 11 Probable locations of the four traffic congestion levels in the city of Zurich.

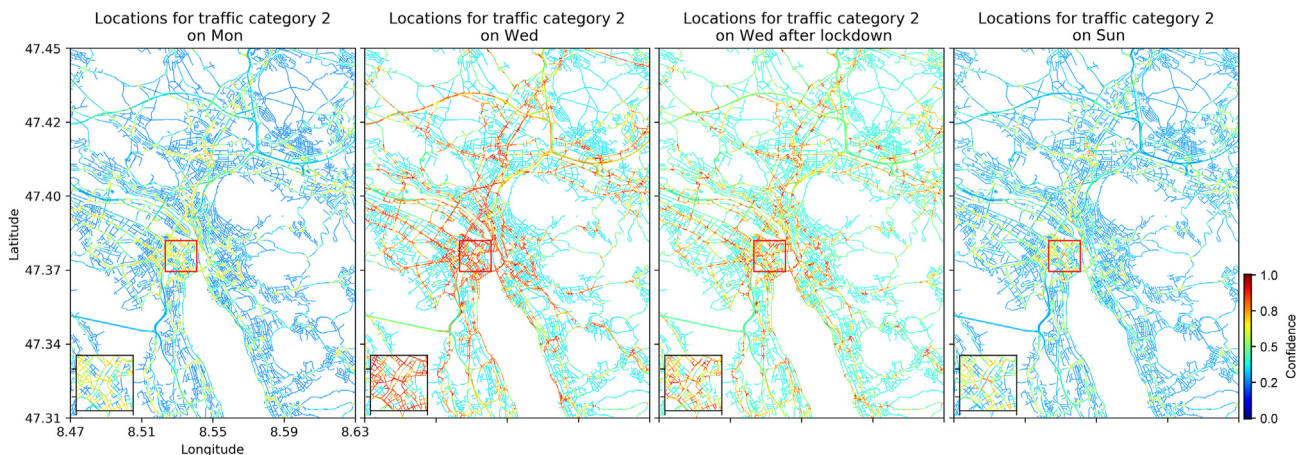


Fig. 12 Probable locations of heavy traffic congestions in different days of a week.

Fig. 11 shows the prediction of the probable locations of the four traffic congestion levels in the city of Zurich. As seen in the figure, all road segments have a high probability of having low traffic density. In contrast, heavy traffic is only expected on individual road segments on the highways or near the city center. Comparing these two levels, intermediate traffic congestions are more likely to happen on all the major roads than the rest of the areas of the city. **Fig. 12** shows the prediction results with the traffic congestion level and the datetime specified. The prediction suggests that heavy traffic is more likely to happen in the middle of a week than at the beginning or the end of a week. Moreover, this trend holds true even in a country-level lockdown.

6. Conclusion

This study presented a pipeline of urban traffic modeling and pattern recognition using SOM. The study took advantage of the increasingly available real-time traffic data from online map vendors, and demonstrated that such data could be used as an alternative to publicly released datasets to scale up traffic modeling to multiple cities. This work also proposed two experiments based on the collected traffic data, and the experiments showed that a rich family of traffic patterns could be detected from multiple cities. Moreover, the study showed that similar traffic patterns existed not only within the same city but also among different cities. This pattern-level similarity revealed a new layer of information for urban planning and urban management. In addition, the experiments demonstrated that various types of traffic predictions can be conducted on the basis of the recognized patterns. Urban planners can search for the typical traffic of a city at specific datetimes or, reversely, ask for the most probable locations of certain traffic patterns.

Meanwhile, the major drawback of the study is that the collected traffic data have already been pre-classified into several categories. Hence, exact traffic flow data, such as velocities and densities, are impossible to retrieve. Thus,

the pipeline presented in this study cannot be easily integrated into conventional traffic models, such as microscopic and macroscopic models. The results are also not well comparable with other data-driven studies based on observational data. Nevertheless, considering their spatial and temporal availability, pre-classified traffic data from online map vendors are still valuable data sources that require further investigation. An interesting direction for future works would be correlating these pre-classified data with raw observational data from local authorities, which would potentially allow us to impute realistic observational data using pre-classified data for areas where observational data are not available.

Declaration of competing interest

The authors declare that they have no known competing financial interests or personal relationships that could have appeared to influence the work reported in this paper.

Acknowledgement

The author would like to thank Dr. Vahid Moosavi, Dr. Diana Alvarez-Marin, and Dr. Karla Saldaña Ochoa for providing valuable suggestions and comments during the study. This study was funded by the China Scholarship Council Grant No. 201706090254.

Appendix

Figure A.1 and **Figure A.2** show the traffic network rendering of the other 31 cities involved in this study. These networks were rendered using the same method of the traffic network shown in **Fig. 5**. As seen, the traffic pattern distribution varies in different cities. But a general conclusion is that, for most cities, a country-level lockdown affects more on the traffic flows in regional highways than in other roads. The highways are also more likely to have a significant traffic flow difference between weekdays and

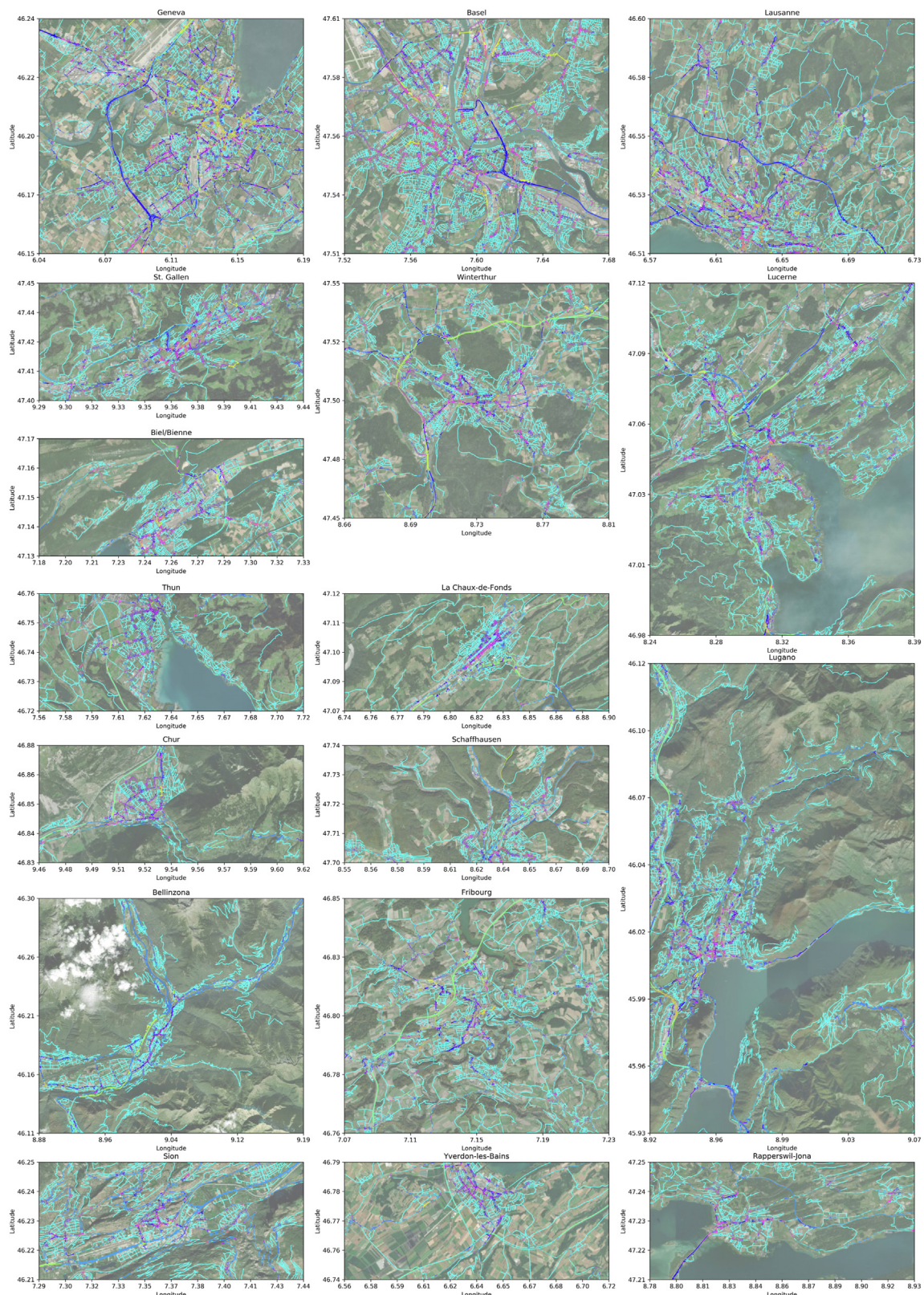


Fig. A. 1 Rendering the traffic networks of multiple swiss-cities based on the traffic flow patterns learnt from the collected data, part 1.

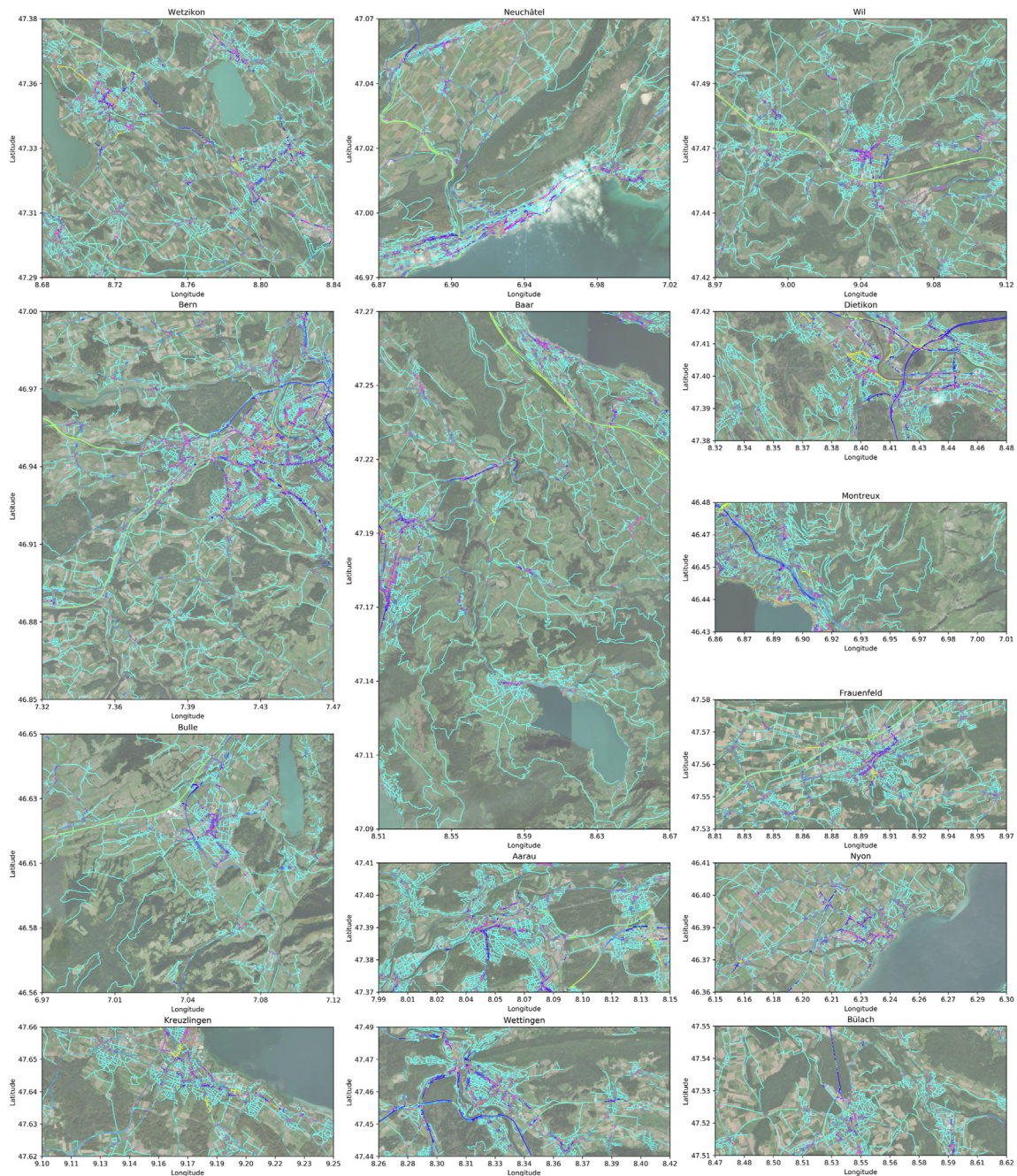


Fig. A. 2 Rendering the traffic networks of multiple swiss-cities based on the traffic flow patterns learnt from the collected data, part 2.

weekends. In contrast, arterial roads that are close to city centers are more likely to have uniform traffic flows in different days. Other road segments, regardless their locations in the city, are less likely to face significant traffic congestions.

References

- Ahmazai, F., 2020. Analyses and modeling of urban land use and road network interactions using spatial-based disaggregate accessibility to land use. *Journal of Urban Management* 9 (3), 298–315.
 Ahmadzai, F., Rao, K.L., Ulfat, S., 2019. Assessment and modelling of urban road networks using Integrated Graph of Natural Road

Network (a GIS-based approach). *Journal of Urban Management* 8 (1), 109–125.

Aw, A.A.T.M., Rascle, M., 2000. Resurrection of "second order" models of traffic flow. *SIAM J. Appl. Math.* 60 (3), 916–938.

Bafna, S., 2003. Space syntax: a brief introduction to its logic and analytical techniques. *Environ. Behav.* 35 (1), 17–29.

Bando, M., Hasebe, K., Nakayama, A., Shibata, A., Sugiyama, Y., 1995. Dynamical model of traffic congestion and numerical simulation. *Phys. Rev.* 51 (2), 1035.

Batty, Michael, 2008. The size, scale, and shape of cities. *Science* 319, 769–771. <https://doi.org/10.1126/science.1151419>.

Brunauer, R., Schmitzberger, N., Rehrl, K., 2018, November. Recognizing spatio-temporal traffic patterns at intersections

- using self-organizing maps. In: Proceedings of the 11th ACM SIGSPATIAL International Workshop on Computational Transportation Science, pp. 43–52.
- Chen, Y., Zhang, Y., Hu, J., Yao, D., 2006, September. Pattern discovering of regional traffic status with self-organizing maps. In: 2006 IEEE Intelligent Transportation Systems Conference. IEEE, pp. 647–652.
- Chen, Y., Zhang, Y., Hu, J., 2008. Multi-dimensional traffic flow time series analysis with self-organizing maps. *Tsinghua Sci. Technol.* 13 (2), 220–228.
- Cremer, M., Ludwig, J., 1986. A fast simulation model for traffic flow on the basis of Boolean operations. *Math. Comput. Simul.* 28 (4), 297–303.
- Edie, L.C., 1965. Discussion of traffic stream measurements and definitions. In: The 2nd International Symposium on the Theory of Traffic Flow, pp. 139–154.
- Endarnoto, S.K., Pradipta, S., Nugroho, A.S., Purnama, J., 2011, July. Traffic condition information extraction & visualization from social media twitter for android mobile application. In: Proceedings of the 2011 International Conference on Electrical Engineering and Informatics. IEEE, pp. 1–4.
- Esser, J., Schreckenberg, M., 1997. Microscopic simulation of urban traffic based on cellular automata. *Int. J. Mod. Phys. C* 8 (5), 1025–1036.
- Evans, M.R., Grimm, V., Johst, K., Knuutila, T., De Langhe, R., Lessells, C.M., Wilkinson, D.J., 2013. Do simple models lead to generality in ecology? *Trends Ecol. Evol.* 28 (10), 578–583.
- Evans, M.R., Benton, T.G., Grimm, V., Lessells, C.M., O’Malley, M.A., Moustakas, A., Weisberg, M., 2014. Data availability and model complexity, generality, and utility: a reply to Lonergan. *Trends Ecol. Evol.* 29 (6), 302–303.
- Ewing, R., Tian, G., Lyons, T., 2018. Does compact development increase or reduce traffic congestion? *Cities* 72, 94–101.
- Gipps, P.G., 1981. A behavioural car-following model for computer simulation. *Transp. Res. Part B Methodol.* 15 (2), 105–111.
- Google, 2020. Map and Tile Coordinates. Accessed from: <https://developers.google.com/maps/documentation/javascript/coordinates> (last access 2020-12-08).
- Hamilton-Baillie, B., 2004. Urban design: why don’t we do it in the road? Modifying traffic behavior through legible urban design. *J. Urban Technol.* 11 (1), 43–62.
- Härri, J., Filali, F., Bonnet, C., Fiore, M., 2006, September. VanetMobiSim: generating realistic mobility patterns for VANETs. In: Proceedings of the 3rd International Workshop on Vehicular Ad Hoc Networks, pp. 96–97.
- Hasan, S., Schneider, C.M., Ukkusuri, S.V., González, M.C., 2013. Spatiotemporal patterns of urban human mobility. *J. Stat. Phys.* 151 (1), 304–318.
- Hillier, B., Leaman, A., Stansall, P., Bedford, M., 1976. Space syntax. *Environ. Plann. Plann. Des.* 3 (2), 147–185.
- Hillier, B., Penn, A., Hanson, J., Grajewski, T., Xu, J., 1993. Natural movement: or, configuration and attraction in urban pedestrian movement. *Environ. Plann. Plann. Des.* 20 (1), 29–66.
- Knospe, W., Santen, L., Schadschneider, A., Schreckenberg, M., 2004. Empirical test for cellular automaton models of traffic flow. *Phys. Rev.* 70 (1), 016115.
- Kohonen, T., 1982. Self-organized formation of topologically correct feature maps. *Biol. Cybern.* 43 (1), 59–69.
- Konieva, K., Knecht, K., Koenig, R., 2019. Collaborative large-scale urban design with the focus on the agent-based traffic simulation. In: Proceedings of the 24th International Conference of the Association for Computer-Aided Architectural Design Research in Asia (CAADRIA) 2019, vol. 2, pp. 221–230.
- Krajzewicz, D., Hertkorn, G., Rössel, C., Wagner, P., 2002. SUMO (Simulation of Urban MObility)-an open-source traffic simulation. In: Proceedings of the 4th Middle East Symposium on Simulation and Modelling (MESM2002), pp. 183–187.
- Laña, I., Olabarrieta, I.I., Vélez, M., Del Ser, J., 2018. On the imputation of missing data for road traffic forecasting: new insights and novel techniques. *Transport. Res. C Emerg. Technol.* 90, 18–33.
- Laña, I., Lobo, J.L., Capecci, E., Del Ser, J., Kasabov, N., 2019. Adaptive long-term traffic state estimation with evolving spiking neural networks. *Transport. Res. C Emerg. Technol.* 101, 126–144.
- Lighthill, M.J., Whitham, G.B., 1955. On kinematic waves II. A theory of traffic flow on long crowded roads. *Proc. Roy. Soc. Lond. Math. Phys. Sci.* 229 (1178), 317–345.
- Montanino, M., Punzo, V., 2015. Trajectory data reconstruction and simulation-based validation against macroscopic traffic patterns. *Transp. Res. Part B Methodol.* 80, 82–106.
- Noulas, A., Scellato, S., Lambiotte, R., Pontil, M., Mascolo, C., 2012. A tale of many cities: universal patterns in human urban mobility. *PloS One* 7 (5), e37027.
- Rakha, H., Hellinga, B., Van Aerde, M., Perez, W., 1996. January). Systematic verification, validation and calibration of traffic simulation models. In: 75th Annual Meeting of the Transportation Research Board, Washington, DC.
- Ratti, C., 2004. Space syntax: some inconsistencies. *Environ. Plann. Plann. Des.* 31 (4), 487–499.
- Richards, P.I., 1956. Shock waves on the highway. *Oper. Res.* 4 (1), 42–51.
- Sakai, T., Kawamura, K., Hyodo, T., 2019. Evaluation of the spatial pattern of logistics facilities using urban logistics land-use and traffic simulator. *J. Transport Geogr.* 74, 145–160.
- Sewall, J., Wilkie, D., Lin, M.C., 2011, December. Interactive hybrid simulation of large-scale traffic. In: Proceedings of the 2011 SIGGRAPH Asia Conference, pp. 1–12.
- Shi, F., 2019. Improving urban non-motorized mobility for public affairs trips: a survey and analysis of innovative official bicycles in Nanjing city, China. *Journal of Urban Management* 8 (3), 396–407.
- Spiliopoulou, A., Kontorinaki, M., Papageorgiou, M., Kopelias, P., 2014. Macroscopic traffic flow model validation at congested freeway off-ramp areas. *Transport. Res. C Emerg. Technol.* 41, 18–29.
- Spiliopoulou, A., Papamichail, I., Papageorgiou, M., Tyrinopoulos, Y., Chrysoulakis, J., 2015. Macroscopic traffic flow model calibration using different optimization algorithms. *Transportation Research Procedia* 6, 144–157.
- Takatsuka, M., Bui, M., 2010. Parallel batch training of the self-organizing map using OpenCL. In: International Conference on Neural Information Processing. Springer, Berlin, Heidelberg, pp. 470–476.
- Wang, S., Yu, D., Ma, X., Xing, X., 2018. Analyzing urban traffic demand distribution and the correlation between traffic flow and the built environment based on detector data and POIs. *European Transport Research Review* 10 (2), 50.
- Weckert, S., 2020. Google Map Hacks. Accessed from: <http://simonweckert.com/googlemapshacks.html> (last access 2020-12-08).
- Wong, G.C.K., Wong, S.C., 2002. A multi-class traffic flow model—an extension of LWR model with heterogeneous drivers. *Transport. Res. Pol. Pract.* 36 (9), 827–841.
- Yuan, Y., Raubal, M., 2012, September. Extracting dynamic urban mobility patterns from mobile phone data. In: International Conference on Geographic Information Science. Springer, Berlin, Heidelberg, pp. 354–367.
- Zonoozi, M.M., Dassanayake, P., 1997. User mobility modeling and characterization of mobility patterns. *IEEE J. Sel. Area. Commun.* 15 (7), 1239–1252.